Tellus (1997), 49A, 371–387
Printed in UK – all rights reserved

TELLUS
ISSN 0280–6495

Rôle of the oceanic heat transport in climate dynamics A sensitivity study with an atmospheric general circulation model

By EMMANUELLE COHEN-SOLAL[1]* and HERVÉ LE TREUT[2], [1]*Program for Climate Model Diagnosis and Intercomparison, Lawrence Livermore National Laboratory, L-264, P.O. BOX 808, Livermore, CA 94550, USA,* [2]*Laboratoire de Météorologie Dynamique du CNRS, École Normale Supérieure, 24 rue Lhomond, 75231 Paris cedex 05, France*

(Manuscript received 21 July 1995; in final form 1 November 1996)

ABSTRACT

Estimating meridional ocean heat transport from the present generation of atmospheric general circulation models, assuming energetic equilibrium, leads to a large variety of results, depending on the model. The current uncertainty on such an important process may cause significant errors in coupled atmosphere/ocean models. To determine the possible nature of these errors, we investigate how the prescription of the oceanic heat transport can affect the results of a coupled surface ocean/atmosphere model where the ocean is limited to thermodynamics and turbulent fluxes but sea-ice is included. In particular, we study the response of the surface fluxes and atmospheric transport to a reduction of the ocean transport. We focus on the initial phase, where these feedback effects begin to develop while the model is still realistic. The model response is strongly dependent on a combination of features: changes in the Hadley cell circulation, the atmospheric heat transport, the radiative and turbulent fluxes at the surface, changes of the radiative fluxes at the top of the atmosphere. In this study, we examine the partitioning between these different effects. It is shown that the atmosphere partly takes up the missing ocean transport, but that this leads to a change in the cloud/radiative equilibrium of the ITCZ region.

1. Introduction

Absorption of solar radiation exceeds outgoing longwave radiation emerging from the atmosphere in the intertropical region, whereas poleward of 40° of latitude the contrary is true. This meridional distribution of radiative heating implies, over long periods of time, a compensating poleward transport of heat by the atmosphere and the ocean. We can derive this global meridional transport of energy from satellite observations, assuming that the climatic system is nearly energetically balanced, although existing measurements show the limits of this assumption. For instance, the Earth Radiation Budget Experiment (ERBE) measurements exhibit an imbalance between the global longwave cooling and the global short wave warming of the system which is estimated as 4.1 Wm^{-2} for the year 1988 (Trenberth and Solomon, 1994). But note that instrument uncertainties may be larger than this estimation.

Moreover, the partioning between the atmosphere and ocean contributions to the meridional heat transport of the climate system is not well known and there remain even greater uncertainties on these separate terms. Atmospheric energy transport can be obtained from the temperature,

* Corresponding author.
email: ecohen@pcmdi.llnl.gov.

geopotential, moisture and wind fields. These fields are obtained from radiosonde data and ship surface marine observations like those used in Oort and Peixoto (1983) and Savijärvi (1988). They may also be derived from atmospheric model analyses such as the European Centre for Medium Range Weather Forecasts (ECMWF) system (cf. Boer, 1986; Masuda, 1988; Michaud and Derome, 1991; or more recently Trenberth and Solomon, 1994). It is often assumed that these atmospheric estimations are reliable enough to derive an estimation of the oceanic heat transport, by substracting atmospheric energy transport estimates from global energy transport estimates deduced from satellites. However, this "residual" method accumulates the errors of each atmospheric measure in the oceanic term and, as stressed by several authors (Holopainen and Fortelius, 1986; Boer, 1986; Gleckler, 1993), the induced uncertainties in the direct computation of the atmospheric energy transport are not well quantified and probably larger than generally recognized. Consequently, they prevent any error bar estimation on the oceanic term. Trenberth and Solomon (1994) propose to improve the residual method by using additional physical constraints. In particular, they adjust the implied oceanic transport by correcting for spurious non-zero net land surface heating implied by the data for long term analyses. After combining ERBE data with the ECMWF atmospheric analyses Trenberth and Solomon obtain a better compatibility with the direct oceanic estimates. Nevertheless, uncertainties in the Southern Hemisphere remain large because of a lack of direct oceanic observations.

Annual mean ocean heat transport may also be deduced from the ocean surface energy budget if one assumes that the heat storage in the ocean over the year is small. The meridional transport is obtained by the pole-to-pole integration of the surface heat fluxes. With this method errors propagate rapidly; a global imbalance of the surface heat budget gives a spurious polar heat transport and makes uncertain even the sign of the heat transport in particular in the Southern Ocean. Despite this, the qualitative features of northward transport poleward of 30N and southward global ocean heat transport in the Southern Hemisphere are intriguing. The only way to minimize the error bars is to improve the quality of the surface heat budget (Hastenrath, 1980, 1982; Hsiung, 1985) but even in regions where the geographical and temporal cover is good there exist large uncertainties and biases (Michaud and Lin, 1992).

The most accurate estimations of the ocean heat transport are the direct measurements based on hydrographic transects (Bennett, 1978; Bryden and Hall, 1980; Bryden et al., 1991; Du, 1981, 1986; Roemmich, 1987; Wunsch and Hu, 1983). These estimations may be more accurate than their atmospheric counterparts, at least in the Northern Hemisphere, and their use has even been suggested to validate the estimations of the atmospheric energy transport (Gleckler, 1993). But these direct oceanographic observations, although consistent, are very sparse and do not provide a global coverage of the oceans. In any case, the intensity of the oceanic transport is expected to be of the same order as the atmospheric heat transport (Trenberth and Solomon, 1994; Carissimo et al., 1985) even though the Carissimo et al. estimation might be slightly overestimated (Covey, 1988).

The above uncertainties on the ocean heat transport may considerably affect the design and validation of coupled atmosphere/ocean models in a manner which requires investigation. When coupled to an ocean which does not transport enough heat, the atmosphere may react by transporting more heat, or through modified fluxes at the top of the atmosphere that will change the total heat transport by the atmosphere and the ocean and the energetics of the climate system. The balance between these two effects is not obvious to predict. We propose to study this problem, at least during the initial phase (10 years) after a transport perturbation occurs, through a simple sensitivity experiment. Fig. 1 provides an illustration of the questions we adress in this study.

The model used in this study is a version of the Laboratoire de Météorologie Dynamique (LMD) atmospheric general circulation model (AGCM) coupled to an upper ocean model. The oceanic component represents the essential physical processes of the surface ocean, such as the vertical turbulence and the sea ice thermodynamics, but does not predict horizontal or large scale vertical velocity. Consequentally horizontal heat transport is not predicted and thus its effect on the geographical redistribution of heat must be prescribed. Oceanic heat transport may be seen as an external parameter, while the atmospheric heat transport can adapt itself to the simulation. This should be

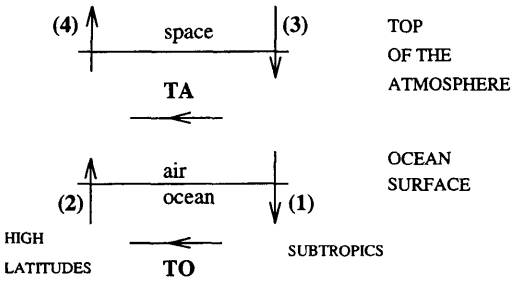

Fig. 1. Schematic of the competition between the ocean and the atmosphere in the climatic system energetics. T_O represents the oceanic heat transport, T_A, the atmospheric energy transport, (1) and (2) are the surface heat budget for the ocean respectively for the subtropics and the high latitudes; (3) and (4) are the net radiative budget at the top of the atmosphere for the same areas.

taken into account when we examine the competition between these two transport processes. We propose two scenarios: one where the ocean transport is diagnosed from the surface fluxes of the uncoupled atmosphere model, and the other where it is assumed to be zero. This drastic sensitivity experiment is justified considering the large range of ocean transport estimates from state-of-the-art AGCM surface fluxes, as demonstrated by Gleckler et al. (1995).

2. Description of the model

We use a coupled model where the atmosphere is a global general circulation model, the LMD AGCM, and the sea ice-ocean model is restricted to the thermodynamics and turbulent dynamics of the upper ocean layers. The model is forced by a seasonal insolation.

2.1. The atmospheric general circulation model

The general design of the LMD atmospheric general circulation model was first described by Sadourny and Laval (1984). The model is a grid-point model with 11 σ-levels unevenly distributed in the vertical. The horizontal discretization is regular in longitude and in sine of the latitude. The resulting equal-area grid cells lead to a coarse latitudinal description of polar regions and a finer one in the tropics, contrary to the zonal discretization being finer at high latitudes. The solar part of the radiative scheme is an improved formulation of the code described by Fouquart and Bonnel (1980); the infrared part is that of Morcrette (1991). Both are the same as the radiative codes presently used in the operational model of the European Centre for Medium Range Weather Forecasts. The version of the LMD GCM considered here, which is called cycle 4, includes a consistent treatment of clouds and radiation based on a prognostic equation for the liquid water (Le Treut and Li, 1991). Sink and source terms are calculated through three schemes: a scheme for non-convective precipitation, including a statistical representation of subgrid-scale condensation; for cumulus convection a scheme of the Kuo-type, and a moist adiabatic scheme are used sequentially. Turbulent fluxes in the boundary layer are computed using diffusion coefficients which depend on the wind shear and thermal stability in the air column, but the evaporation and the sensible heat from the ground are crudely parameterized since the drag coefficient used in the bulk formulas depends on season and ground nature (sea or land) only. The parameterization of land-surface processes used in this cycle 4 version of the LMD GCM is also simple (Laval et al., 1981) since the ground temperature and soil moisture are computed for a single ground layer. This is consistent with the fact that the diurnal cycle of solar insolation is not taken into account but the seasonal cycle is. Further versions of the model include a more advanced vegetation scheme (Ducoudré et al., 1993). Surface albedo over land is prescribed according to Schutz and Gates (1972). The ice cover is allowed to cover a fraction of a grid cell, but the ice and snow albedo (nominal value fixed at 80%) depends on the solar zenithal angle only. A dependence of the snow albedo on the vegetation cover, the age of the snow, and the surface melting conditions has been introduced into a later version of the LMD model (Chalita and Le Treut, 1994). The contribution of the snow on the sea ice thermodynamics is not considered here. These assumptions, however, are expected to have a limited impact on our sensitivity studies, since they only affect the ocean indirectly.

2.2. The oceanic mixed layer model

The mixed-layer model is based on a formulation proposed by Garwood (1977). It was modified

by Gaspar (1988) who introduced a new parameterization of the turbulent dissipation to account for rotation and stability constraints, quantified respectively by the Ekman length scale (λ) and the Monin-Obukhov length (L). The advantage of this formulation is that the necessary coefficients have been calibrated independently from the test performed at the ocean weather station Papa, which served to validate the model. The entrainment at the base of the mixed layer is evaluated from budgets of the total turbulent kinetic energy (TKE) and its vertical component. The condition for entrainment is that the total supply of TKE must be greater than a minimal value computed from the oceanic mixed layer characteristics and the forcing. When the entrainment condition is not satisfied, a retreat of the boundary layer base occurs; this is defined by the instantaneous adjustment of the mixed layer depth (h) at a lower value so as to maintain the TKE at its minimal value, $h=mL$, where m is a function of h/λ and h/L. In the model, the boundary layer is a totally mixed layer.

Below this mixed layer, the pycnocline is described down to 800 m by a maximum of 20 layers unevenly distributed on the vertical. A thick bottom layer, from 240 to 800 m, is used to damp the variations of temperature and salinity induced by deep reaching entrainment events.

The determination of the oceanic mixed layer depth together with heat and salt conservation laws closes the calculation of the oceanic temperatures and salinities for the 20 layers. There are two kinds of sink and source terms for these budget equations: The first are the fluxes resulting from the atmosphere/ocean heat and water exchanges. The heat flux is totally absorbed in the mixed layer, except a part of the solar radiation that penetrates more deeply in the ocean below the mixed layer according to a law proposed by Paulson and Simpson (1977). The second kind of source and sink terms are the fluxes induced by the variations of the mixed layer depth. When entrainment occurs, heat and water turbulent fluxes are exchanged at the base of the mixed layer. In the case of retreat, the conservation of potential energy within the column of water (Adamec et al., 1981) imposes again salinity and temperature fluxes between the mixed layer and the layer below.

The model requires a stable stratification of the oceanic column, and thus an additional mixing from the surface to deeper layers may occur for unstable stratifications. There is no added diffusion in the model and the only mixing processes are those within the mixed layer.

2.3. *The sea-ice model*

The sea-ice model is thermodynamic only. It predicts the thickness and the compactness of the ice cover. Following a simple sea-ice model described by Semtner (1976), it is based on a "zero-layer" heat budget for the ice. The snow cover effect is neglected. In addition, the fraction of open water (or lead) is allowed to vary assuming a two-level ice thickness distribution as proposed by Hibler (1979). Freezing and melting rates are calculated from local imbalance between the atmospheric and oceanic heat fluxes.

At the atmosphere/ice interface the coupling is totally interactive. The sea-ice surface temperature calculation is included in the boundary layer calculation of the AGCM and is consistent with the turbulent heat fluxes. At the ocean/ice interface the coupling is both thermodynamical (phase equilibrium) and dynamical (turbulence forced by brine rejection). There is no treatment of ice dynamics in the current model.

3. The oceanic heat transport

As no oceanic velocity field can be calculated in the present model, we determine separately the heat transport by the oceanic currents. It is introduced as an additional diabatic term in the equation of temperature for the oceanic surface mixed layer (of depth h). This temperature, which is also the sea surface temperature (and therefore referred as SST) is computed through a heat budget equation, involving the surface heat fluxes, the heat exchange at the mixed layer base and the part of the solar radiation which is absorbed within the mixed layer. The equation reads:

$$\rho_0 c_p h \frac{\partial T_m}{\partial t} = -\rho_0 c_p w_e \Delta T + SW_{sfc}\,[1-I(-h)] - (LW_{sfc}+LE+H)+\rho_0 c_p h \frac{\partial T}{\partial t_{adv}}, \quad (1)$$

where ρ_0 is the constant oceanic density (Boussinesq approximation), c_p the specific heat of oceanic water, T_m the sea surface temperature, t the time, w_e the entrainment velocity of the mixed layer base (defined positive when h increases), ΔT the temperature step between the bottom of the mixed layer and the underlying thermocline, SW_{sfc} the net solar radiation at the surface, and $[1-I(-h)]$ the fraction of the solar flux absorbed within the mixed layer. The terms LW_{sfc}, LE and H are respectively the longwave net radiation, the latent heat and the sensible heat fluxes at the surface of the ocean. The last term in eq. (1) represents the thermodynamical impact of the heat transport convergence on the SST rate of variation:

$$\rho_0 c_p h \frac{\partial T}{\partial t_{adv}} = -\mathrm{div}(T_O). \quad (2)$$

Note that this term is entirely applied within the oceanic mixed layer which means that the deep transport of heat is neglected. In addition, this term is chosen to be evenly distributed during the year (no seasonal cycle) but it is not uniform in space, as explained below.

3.1. *Determination of div(T_O) and T_O*

In order to diagnose the oceanic heat transport, climatological annual means are considered so that the surface ocean heat storage can be neglected. Surface heat fluxes into the ocean balance the heat transport divergence as follows:

$$\overline{\mathrm{div}(T_O)} = \overline{SW_{sfc} - LW_{sfc} - LW - H}. \quad (3)$$

The overbar represents the temporal mean at each grid point.

In this study, the estimation of the oceanic heat transport is obtained using the surface heat fluxes entering the ocean computed by the LMD AGCM from an eight year simulation. This AGCM run (hereafter called ATMO) uses prescribed climatological SSTs and sea ice cover.

The diagnosed heat transport divergence is shown in Fig. 2. In annual mean, the non solar heat fluxes tend to cool the ocean and thus are negative. The only exception appears in high latitudes where the sensible heat flux is slightly positive. The largest oceanic heat losses are found east of the Northern continents, and result from continental air masses flowing over warm oceanic currents. Latent and sensible heat losses are largest in the Gulf Stream and Kuroshio currents. In subsidense areas, the surface heat flux loss can also be large because of the latent heat loss absorbed by the dry air coming from the descending branch of the Hadley circulation. On the contrary, the equatorial latitudes mostly gain heat because of a large insolation and a reduced latent heat flux due to the high level of atmospheric humidity limiting the evaporation at the surface.

Fig. 3 reproduces the zonal and annual average

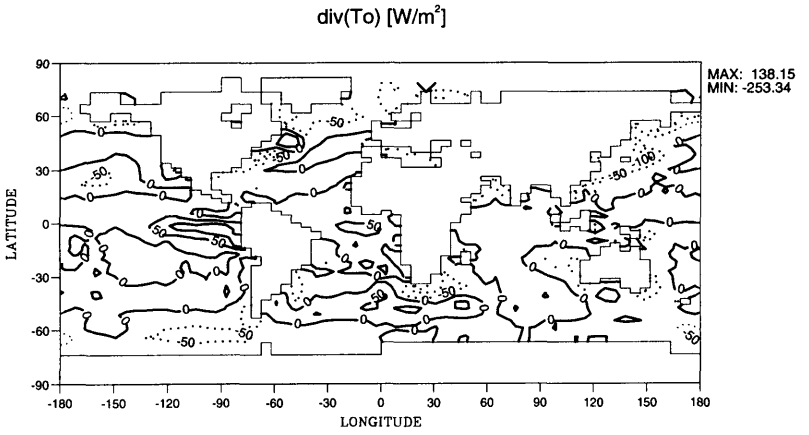

Fig. 2. 8-year mean ocean surface heat flux simulated by ATMO (simulation performed with the LMD uncoupled AGCM). This term is used as the oceanic heat transport divergence in the simulations performed with our coupled model.

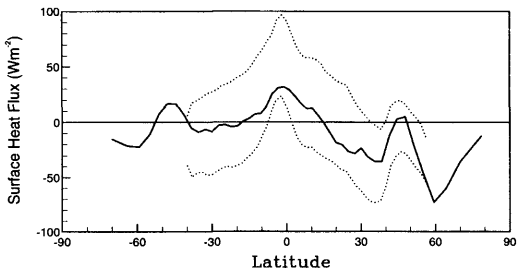

Fig. 3. Zonal and annual average of the ocean surface heat flux as simulated by ATMO (uncoupled AGCM, 8 yrs) is given by the solid line. Dotted lines represent observational error bounds from Gleckler and Weare (1996).

of the ocean surface heat flux compared to observational error bounds (Gleckler and Weare, 1996). In the subtropics, the warming corresponds to the lower error bound and consequently is not very strong, whereas at midlatitudes the heat budget becomes positive again. Therefore, the meridional gradient is weaker than in the data.

The heat transport through a vertical latitudinal wall in the oceans at the latitude ϕ is computed by the integration of its zonal mean divergence (Fig. 3) from the south pole Antarctic coast (SP) to the latitude ϕ for the oceanic points only. We assume that $\mathrm{div}(T_O)$ is equal to 0 on the continents:

$$T_O(\phi) = \int_{SP}^{\phi} \left(\int_{-\pi}^{\pi} \mathrm{div}(T_O)(\phi, \lambda) a \, d\lambda \right) a \cos(\phi') \, d\phi', \tag{4}$$

where λ represents the longitude and a the Earth radius. The conventions of eq. (4) give a positive value when the meridional heat transport is northward and ensure a null transport at the Southern edge. $T_O(\pi/2)$ represents the accumulated oceanic northward transport at the north pole. Physically this must be zero. The condition to satisfy this constraint is that the net heat flux (or term $\mathrm{div}(T_O)$) averaged over the global ocean be zero.

In the LMD simulations, however, the surface heat budget, in global mean over the oceans, presents an imbalance corresponding to a heat loss for the ocean of about 3.1 Wm^{-2}. If we want to diagnose the effective T_O, we have to correct the spurious nonzero transport at the North Pole. Carissimo et al. (1985) make the comparison of various types of correction to maintain the global balance, when deriving the total heat transport from the radiative budget at the top of the atmosphere. In our case the global imbalance is small, and we use a simple uniform correction (Gleckler et al., 1995). The implied meridional oceanic heat transport computed from the corrected net surface heat flux is shown in Fig. 4. The maximum northward heat transport realistically occurs between 10N and 20N. The value of this maximum is uncertain because it is sensitive to the type of correction, but it is of the same order as the oceanic transport estimations based on various observational data (Hsiung, 1985; Esbensen and Kushnir, 1981; Trenberth and Solomon, 1994) with the exception of the result of Carissimo et al. (1985) which is much larger. In the Southern Ocean, there is a slight southward transport whose amplitude depends on the correction. When the same diagnosis is applied to other AGCMs by Gleckler et al. (1995), they exhibit a large model-to-model variability of the Southern Ocean transports, from over 1.5×10^{15}W southward to over 2×10^{15}W northward, at about latitude 30S. Gleckler et al. (1995) analyze these large discrepancies between the models in term of cloud radiative forcing on the simulated surface shortwave radiation.

In Fig. 4 estimates of the meridional heat transport by basins are also shown. To determine these, the corrected net surface heat flux is integrated

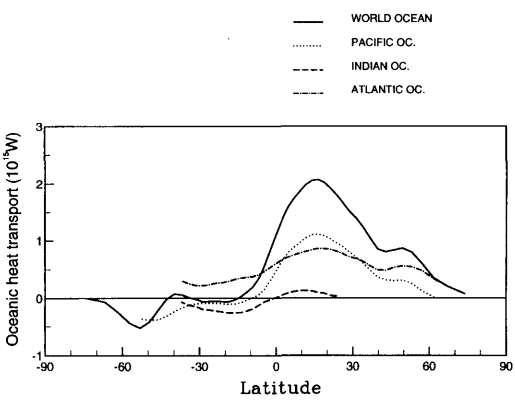

Fig. 4. Annual northward oceanic meridional heat transport (10^{15} W): computed as the integration of the ocean surface heat fluxes simulated by the uncoupled simulation ATMO (8 yrs) for the world ocean (solid line), the Pacific Ocean (dotted line), the Atlantic Ocean (dash-dotted line) and the Indian ocean (dashed line). A standard uniform correction is used for removing the spurious nonzero transport at the poles.

from north to south for each basin. The shapes of the curves are qualitatively in accordance with most other surface flux method estimates: the Atlantic heat transport is northward at each latitude north of 40S and the southward component in the Southern Hemisphere is due to the Pacific and Indian ocean basins contributions.

3.2. *Experimental design*

The purpose of this study is to test the sensitivity of the atmosphere/surface ocean system to a change in the prescribed ocean heat transport. With our simplified coupled model we cannot diagnose feedback effects in which the ocean circulation and the other components of the climate system mutually interact. However, we can study the direct impact of the ocean heat transport on the climate system, and clearly isolate this effect.

For this purpose, we have evaluated the sensitivity of the simulations to this ocean advection term. We present the extreme case which is to use either the term $\mathrm{div}(T_O)$ as described above, or no advection at all. In the experiment control, $\mathrm{div}(T_O)$ is introduced as a diabatic term in the SST equation (eq. (1)); it is constant in time but non-uniformly distributed (Fig. 2). Note that $\mathrm{div}(T_O)$ is taken according to eq. (3) and the correction that was previously necessary to insure a zero global mean is no longer applied. The surface solar radiation, a preponderant term in the surface budget, can contain many errors, mostly because of the uncertain representation of the surface cloud radiative forcing. In the AGCM uncoupled simulations, the simulated climate is on the contrary largely insensitive to the solar radiation which goes through the atmosphere and reaches the surface of the ocean, where the SSTs are prescribed independently. Hence, even if the surface heat flux and therefore the diagnosed oceanic heat transport contain strong anomalies, the uncoupled behaviour of the simulated atmospheric general circulation can be realistic. The problem becomes crucial when the atmospheric model is coupled with an oceanic model, since the anomalies of the surface heat fluxes then directly impact the ocean temperatures. For this reason, contrary to its use in the diagnosis of T_O, the surface heat flux is introduced with no correction in each oceanic grid cell as the local heat transport divergence. Thus, this ocean heat transport term also partly compensates the surface heat flux defaults. In the experiment identified as ADV^0, the oceanic transport term is suppressed from eq. (1).

All experiments are run with the LMD atmospheric general circulation model at a resolution of 64 points in longitude, 50 in sine of the latitude and 11 vertical levels for the atmosphere. The ocean and sea ice interact with the atmosphere once per day. The insolation includes a seasonal cycle but no diurnal cycle.

The horizontal grid cells for the ocean coincide with those for the atmosphere and, vertically, the temperature and the salinity are computed for 20 oceanic layers. The coupled experiments begin on the first of January and are initialized from the Levitus global ocean temperature climatology (Levitus, 1982) interpolated on the 20 vertical layers of the model. The atmospheric initial state is the result of a previous uncoupled simulation of the AGCM and it is the same for all simulations. The sensitivity experiments are analyzed with emphasis on the initial 10-year period as we wish to study the feedback processes in their developing phase, in a regime where the simulations remain quite realistic.

3.3. *Performance of the control simulation*

Some aspects of the control simulation are described in Cohen-Solal and Le Treut (1996); mixed layer depths are realistically simulated and ocean surface temperatures compare well with the observations used to force the uncoupled simulation ATMO. At a longer time scale, the 70-yr control simulation CONTROL undergoes a slight climate drift involving a decrease of the global mean SST of 0.3°C per decade. This occurs with the imposed oceanic heat transport. But the cold drift is small and less pronounced in the beginning of the control simulation. Therefore, by limiting our analysis to the first ten years of the control and sensitivity simulations, our results are not significantly effected by the drift.

4. Results of the experiments

Beyond the direct impact of an ocean circulation change on the SST, our aim is to diagnose the compensating effects by which a change in the oceanic energy transport affects the fluxes at

the ocean/atmosphere interface and the atmospheric energy transport. We first examine SST changes, and then the implications on the ocean/atmosphere coupled energetics.

4.1. *Simulation of the SST*

We first describe the results in terms of SST. Our experiment gives a rough measure of how much the oceanic currents affect the SST distribution, and how resulting errors may affect coupled models.

Fig. 5 shows the evolution over 10 years of the SST difference between the two experiments (ADV^0 − CONTROL) in zonal mean. The seasonal and local characteristics of the difference establish themselves rapidly and are apparently stable at the end of the 10 years.

However, there is still a slower evolution affecting deeper oceanic layers in ADV^0, which is apparent in the surface energy evolution of ADV^0 displayed below (Fig. 6). As noted earlier, neither simulation has attained equilibrium at this time of the simulation. In this report we wish to concentrate on the initial atmosphere and surface ocean feedbacks which occur in response to the removal of the ocean heat transport. This transient phase exhibits a quasi-stable response and is more interesting to us than the steady phase in which the models would establish non-realistic climates.

At high latitudes near the sea ice boundaries the temperature of the ocean is close to −2°C for both simulations. The absence of ocean transport in ADV^0 is mostly felt, in terms of SST, at low latitudes and in the northern midlatitudes (Fig. 5).

Fig. 7 shows the 10-year average difference of SST between ADV^0 and control runs. There is a strong analogy between this figure and the ocean transport term (Fig. 2): the suppression of this term in eq. (1) for ADV^0 has indeed a direct impact on the temperature (warming when there was a divergence of heat and cooling otherwise). The discrepancies between Fig. 7 and Fig. 2 are due to the mixed layer and atmospheric feedbacks.

In Fig. 5 or Fig. 7, ADV^0 shows an increase of the temperature between 15N and 15S, with a maximum around the equator where the heat transport divergence was maximum in control. The difference of temperatures is negative northward of this area. Whereas the temperature gradient is strongly affected in the intertropical areas, it is less changed at midlatitudes.

Fig. 8 represents the difference of atmospheric temperatures between ADV^0 and control in response to the ocean transport perturbation. Between the surface and an altitude of 850 hPa, the difference of air temperature is qualitatively similar to the SST difference (Fig. 7). This is because near the ground the characteristics of the surface are communicated to the atmosphere through the strong turbulence of the atmospheric mixed layer. In higher altitudes, the action of winds and the changes in cloudiness, radiative fluxes and atmospheric circulation, make the

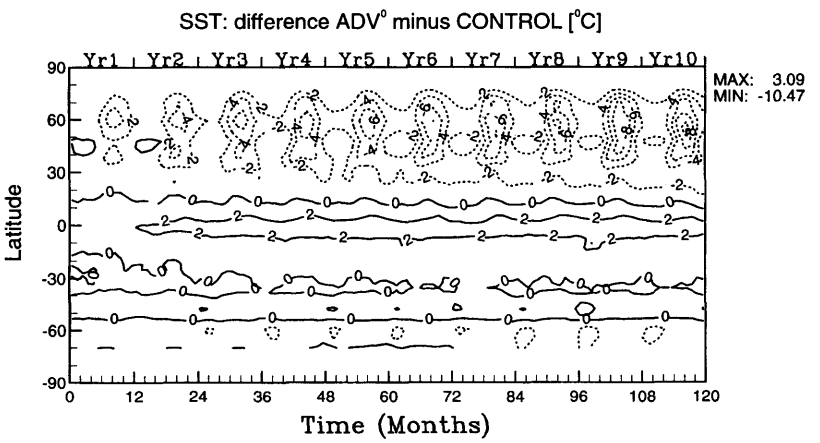

Fig. 5. Time evolution of the difference, in zonal mean, of the ocean surface temperatures (°C) simulated by ADV^0 and CONTROL (ADV^0 minus CONTROL).

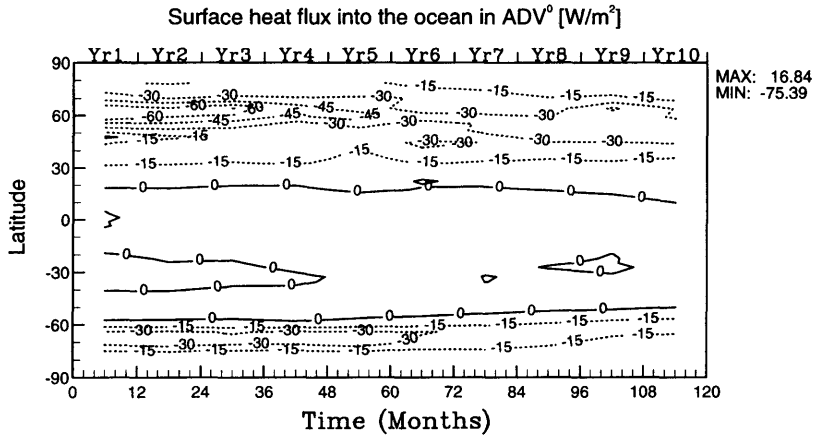

Fig. 6. Time evolution of the net surface heat flux into the ocean (W/m^2) in zonal and annual mean, simulated by ADV^0 for 10 years.

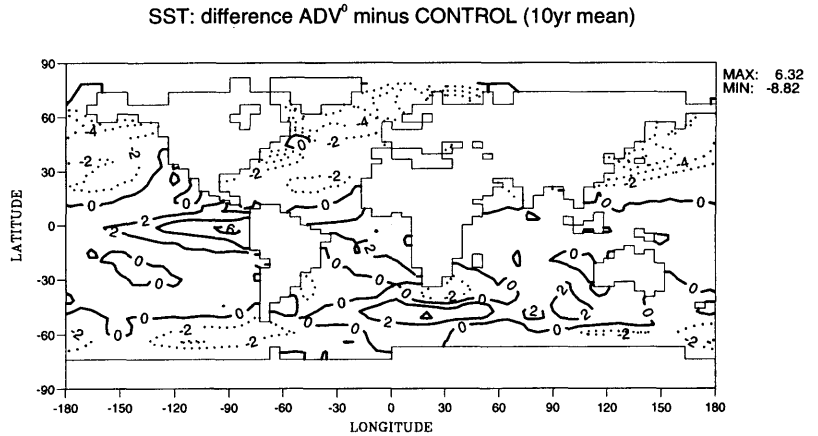

Fig. 7. Annual average over 10-yr simulation of the difference of SST simulated by ADV^0 and CONTROL (ADV^0 minus CONTROL).

higher atmosphere's temperature response more complex. In the troposphere, low latitude surface warming and northern hemisphere cooling tend to extend higher in the atmosphere. But in the Southern Hemisphere, the troposphere is warmer in ADV^0 than in control when the surface shows a cooling. At the top of the atmosphere, for pressure under 200 hPa, the temperature is generally cooler in ADV^0 than in control, independently of the near surface structure.

4.2. *Surface heat fluxes*

The annual mean net surface heat fluxes computed by CONTROL are reproduced in Fig. 9a.

There exists a strong analogy between Fig. 9a and Fig. 2. In contrast, the sensitivity experiment ADV^0 gives quite different results. The net surface heat fluxes computed by ADV^0 are represented in Fig. 9b. The sign of the net surface heat flux entering the ocean is conserved but, very clearly, with lower extremums. In the annual and zonal mean the net heat fluxes into the ocean in the subtropics hardly reaches 6 W/m^2 in ADV^0 while the experiments control and ATMO attain 30 W/m^2 (Fig. 10). This term for ADV^0 must of course reach a zero-value in annual mean when a complete equilibrium is attained, which is not the case after 10 years of simulation as shown by Fig. 6.

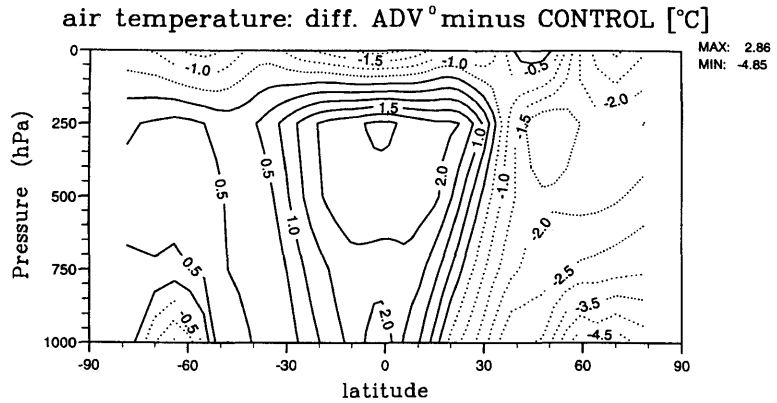

Fig. 8. Zonal and annual (10-year simulation) mean of the difference of the air temperature simulated by ADV^0 and CONTROL (ADV^0 minus CONTROL).

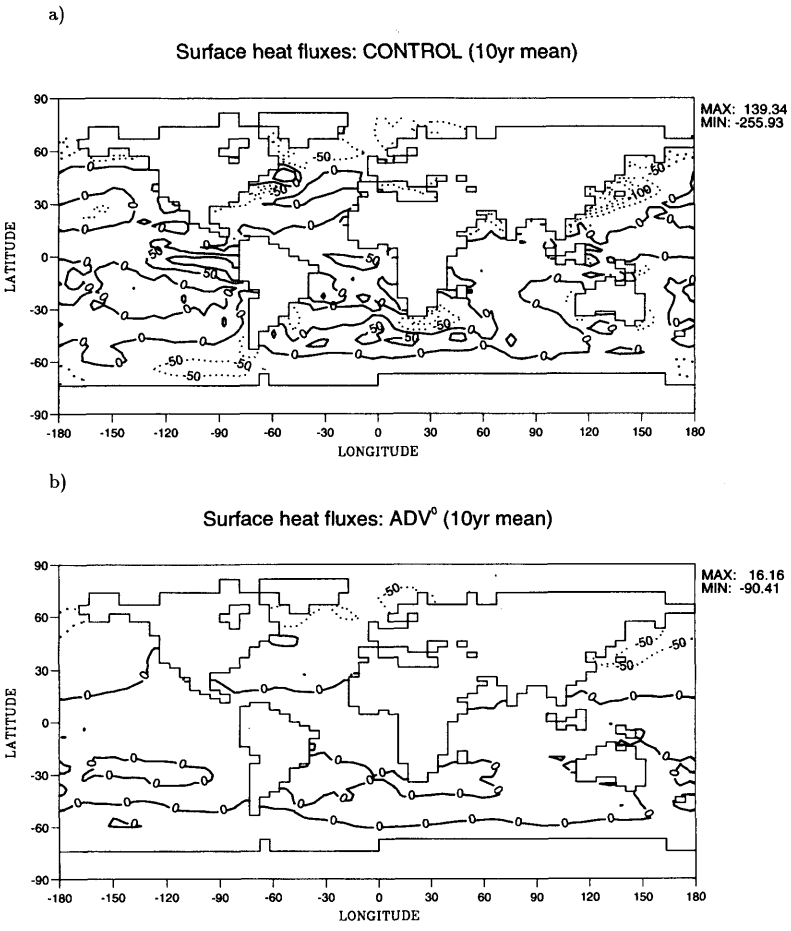

Fig. 9. Surface heat fluxes (W/m^2) into the ocean as simulated by (a) CONTROL and (b) ADV^0, averaged over 10-yr.

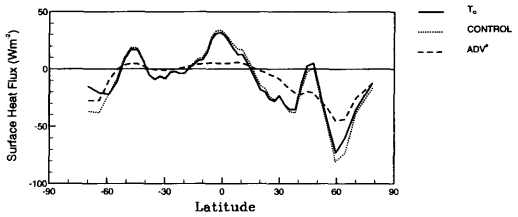

Fig. 10. Zonal and annual mean of the surface heat budget into the ocean (W/M^2) simulated by ATMO (curve T_O, 8-yr mean), CONTROL and ADV^0 (10-yr mean).

The absence of oceanic transport in ADV^0, by decreasing the surface ocean temperature, tends to cut off permanent sources of heat for the atmosphere in the northern midlatitudes (around latitude 30°N) and to a lesser extend around latitude 30°S. In the same time, there is a disapearance of permanent sinks of heat in the equatorial area and at latitude 40°S.

We wish now to study how this evolution toward equilibrium is accomplished. Fig. 11 represents the difference of the total non solar heat fluxes (turbulent heat fluxes plus net infrared radiation) between ADV^0 and CONTROL in annual and zonal mean over the oceans. The general shape of this curve is as expected similar to that of the oceanic heat transport divergence which is suppressed in ADV^0: In the subtropics for instance as the suppressed term corresponds to a cooling, the SST increase and the non solar heat losses increase. The most remarkable exception is at the equator where instead of the expected maximal impact (div(T_O) was maximal here), the non solar heat fluxes do not change significantly. This can be explained by more detailed analyses below.

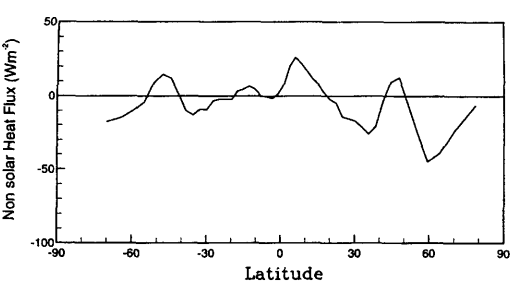

Fig. 11. Zonal and annual mean (10-yr mean) of the simulated total non solar heat flux (W/m^2) over the ocean: difference between the sensitivity experiment ADV^0 and the CONTROL experiment CONTROL (ADV^0 minus CONTROL). A positive value means a heat loss for the ocean.

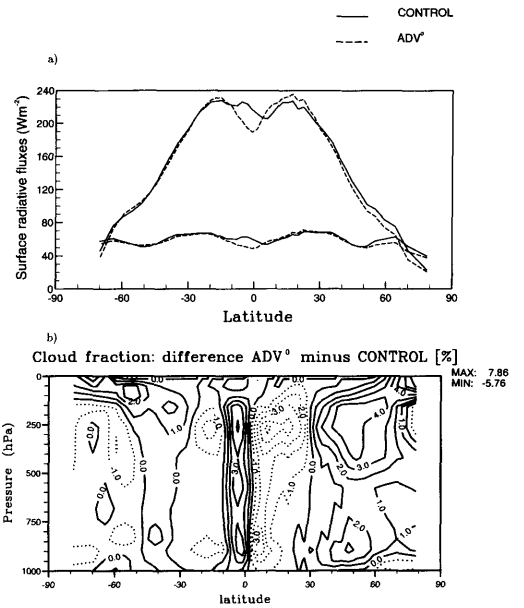

Fig. 12. (a) Zonal and annual mean (10-yr mean) of the net surface shortwave radiation reaching the ocean (upper curves) and the net surface infrared radiation positive when outward from the ocean (lower curves) (W/m^2), simulated by CONTROL (plain curve) and ADV^0 (dashed curve). (b) Zonal and annual mean of the cloud fraction (10-yr mean): difference ADV^0 minus CONTROL. The increase of the nebulosity at the equator and the decreases in the subsidense areas are indicative of a change in the mean circulation.

Fig. 12a represents the surface solar and net infrared fluxes over the ocean for the simulations CONTROL and ADV^0. In the equatorial area, the surface infrared flux decreases in ADV^0 relative to CONTROL. This explains why the sum of the non solar heat fluxes do not change at these latitudes (Fig. 11). It corresponds to an increase of the downwelling atmospheric infrared radiation, whereas the surface emitted radiation also increases since the equatorial temperature is warmer by about 2 degrees. But for ADV^0, in the equatorial area, the surface solar flux decreases (Fig. 12a). This shortwave decrease, and the downwelling longwave increase have a common origin, which is a larger amount of clouds in the convective area (Fig. 12b). The decreased equatorial heat flux (Fig. 10) results from the lower solar radiation (and larger evaporation), whereas the increased downward longwave radiation tends to

enhance the surface warming. The long-wave effect is amplified by the water vapor increase. This latter effect has been referred to as the tropical super greenhouse effect (Ramanathan and Collins, 1991). This competition in low latitudes, between the cloud albedo feedback and the cloud and water vapor greenhouse effects, has already been noted to play an important role on the climate sensitivity as estimated from observations (Ramanathan and Collins, 1991; Lubin, 1994) or from GCMs results (Washington and Meehl, 1993; Meehl and Washington, 1995; Boer, 1993; Le Treut et al. 1994). It is very sensitive to the cloud parameterizations (Meehl, 1995). It is interesting to note that in our model the super greenhouse effect on longwave radiation is not the dominant term, the sign of the result being determined by the changes in the shortwave and latent heat fluxes. Cloud and water feedbacks tend globally to stabilize the system but since the surface heat budget is not equal to zero the SSTs are still increasing in the equatorial ocean at the end of the 10 years under consideration.

The surface ocean modifications induce tropical atmospheric changes. As illustrated below, when we analyze the transport of energy, the Hadley cell is accelerated. This adjustment of the mean circulation is consistent with the increase of the cloud cover in the convective area which we have already noted, and a decrease of the cloud cover in the subsidense areas (Fig. 12b). ADV^0 gives rise to dynamical and convective changes associated with changes in clouds and moisture radiative effects. The link between radiative, dynamical and convective processes in the subtropics is described by Slingo and Slingo (1988) as a feedback at work in their simulations. Randall et al. (1995) essentially found the same feedback using a different AGCM. The framework of these previous studies was quite different from the present one since they used uncoupled AGCMs forced by prescribed SST, in order to compare how the radiative-dynamical-convective feedback evolved when the cloud parameterization was modified (Slingo and Slingo, 1988; Fowler and Randall, 1995). In our case, the ocean is interactive with the atmosphere, and the response is expected to be more complex. In spite of these differences, the radiative-dynamical-convective feedback is again at work. Hence, the interactions between the cloud radiative forcing, the convective activity and the mean circulation are sensitive to any tropical perturbation, whatever its nature, and the model response is not limited to a local radiative response but involves dynamical processes. This may induce a longer adjustment time for atmospheric (or coupled) models.

4.3. *Radiative fluxes at the top of the atmosphere*

The net solar radiation and outward long-wave radiation at the top of the atmosphere simulated by ADV^0 and CONTROL are represented in Fig. 13a. The modifications of the solar flux at the top of the atmosphere have the same properties as those at the surface (Fig. 12a). Both reflect the planetary albedo variations due to cloudiness changes. The contribution of changes in the solar energy absorbed by the atmosphere (obtained as the difference between solar flux at the top of the atmosphere and surface solar flux) remains small and less than 5 W/m^2: this value is found in the

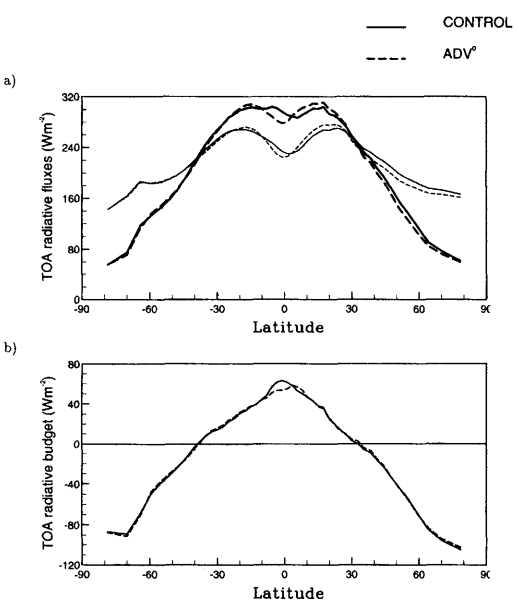

Fig. 13. (a) Zonal and annual mean (10-yr mean) of the net solar radiation (incoming less reflected, in thick lines) and the outward longwave radiation (thin lines) at the top of the atmosphere, simulated by CONTROL (plain curves) and ADV^0 (dashed curves). (b) Same as in (a) but for the net radiative budget at the top of the atmosphere (difference between the net solar radiation and the outward longwave radiation of a).

equatorial region and is due to an increase of the atmospheric water vapor (not shown here).

In addition, the outward long-wave radiation at the top of the atmosphere undergoes changes which are consistent with the effect of clouds on the shortwave radiation (decrease of greenhouse effect when albedo increases). Obviously, the long-wave radiation changes do not fit with the difference of atmospheric temperatures at the top of the atmosphere (Fig. 8) and are directly linked to the changes in cloudiness (Fig. 12b).

As a result of the changes in solar and longwave radiations at the top of the atmosphere, the net radiative budget at the top of the atmosphere is also modified (Fig. 13b): the opposite effects in solar and longwave do not exactly compensate. In particular, in lower latitudes, the effect of the perturbation has a stronger effect on the solar term (it decreases in ADV^0) and results in a smaller positive radiative budget in the sensitivity experiment ADV^0 than in control.

4.4. *The competition between oceanic and atmospheric heat transport*

We have shown that the meridional gradient of air-sea fluxes (Fig. 9b) and the net radiative budget at the top of the atmosphere (Fig. 13b) decrease with the suppression of the oceanic heat transport. In Fig. 1 the terms (1) and (2) decrease as well as (3) (the variations for (4) are slight) when we cut off the term T_O.

The evolution of the term T_A which represents the atmospheric energy transport is complex, because it depends on all these fluxes. The evolution of this atmospheric transport indicates that the climate system is acting to stabilize itself in response to a change in the oceanic transport. This compensating role of the atmosphere when ocean heat transport is modified has also been shown by Covey and Thompson (1989) with an atmospheric model forced by different oceanic boundary conditions corresponding to different amounts of equator-to-pole oceanic heat transport (no atmospheric feedback on the SSTs).

The transport T_A simulated by our model is diagnosed as the meridional transport of the sum of the geopotential gz, the sensible heat $c_{pa}T$ and the latent heat Lq by the total flow, accross a latitudinal circle of latitude ϕ (Michaud and Derome, 1991; Trenberth and Solomon, 1994). The transport of kinetic energy which is always small is neglected in the diagnosis. T_A reads:

$$T_A(\phi) = 2\pi a \cos\phi \int_{sfc}^{toa} \overline{[(c_{pa}T + gz + Lq)V]}\, dz, \tag{5}$$

where toa and sfc mean, respectively, "top-of-the-atmosphere" and "surface", and the brackets represent a zonal average.

Fig. 14 represents the atmospheric energy transport simulated by control and ADV^0. It shows that in the absence of horizontal redistribution of heat by the ocean, the atmosphere at least partially compensates for the missing oceanic contribution. In the lower latitudes and to a lesser extend in the southern midlatitudes, the poleward energy transport is stronger when the oceanic transport is suppressed. The maximal impact corresponds to the location where the northward heat transport by the ocean was also maximum.

The ocean transport decrease at 15°N is about 2×10^{15}W in the ADV^0 experiment, whereas the atmospheric transport increases by 1×10^{15}W on average over the 10 year mean. Although acting to stabilize the meridional gradient of temperature, the increased atmospheric transport does not fully compensate the missing oceanic transport during the 10-year mean. As a consequence the total transport decreases in ADV^0, which is also reflected in the decreased meridional gradient of radiation budget at the top of the atmosphere (Fig. 13b).

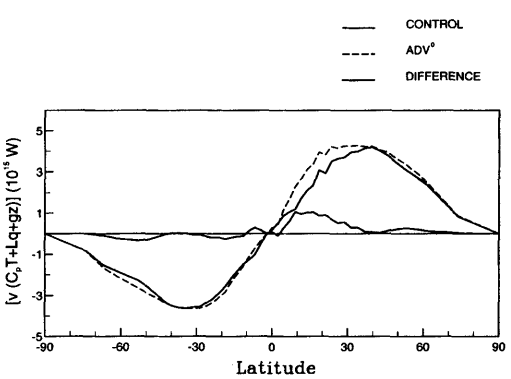

Fig. 14. Zonally and vertically integrated annual meridional transport of atmospheric energy by the total flow in units of 1 PW = 10^{15} W as simulated by the control simulation CONTROL and the sensitivity experiment ADV^0 and their difference, for the 10-yr simulations.

But the change in the radiation at the top of the atmosphere remains small and corresponds to a decrease of the transport of about 0.2×10^{15}W (Fig. 15). Hence in ADV^0, the equator-to-pole gradient of the net radiative budget at the top of the atmosphere does not reflect the actual divergence of heat transport by the global system (i.e., by the atmosphere in ADV^0). That is because of the ocean heat storage: in average over the ADV^0 10-year simulation, the ocean absorbs heat at low latitudes and loses heat at higher latitudes.

As a consequence, the radiative loss at the top of the atmosphere over high latitudes is stronger than it would be at equilibrium, the air temperature meridional gradient is reduced and the average atmospheric heat transport increase is lower that it would be at equilibrium. In Fig. 16, we compare the mean difference in atmospheric transport for the 10-year simulations with the corresponding difference but for the last year of simulation ADV^0 and still the 10-yr mean of CONTROL. It shows that the atmospheric energy transport increases as ADV^0 tends toward equilibrium and tends to compensate more closely the missing oceanic heat transport T_O. But the value of the T_O maximum is sensitive to the correction and the comparison should only be made qualitatively. In this initial phase where equilibrium is not attained the change in the atmospheric transport constitutes a dominant feature.

Fig. 17 shows the repartition of the meridional atmospheric transport, for both experiments, between different terms of energy: geopotential gz, sensible heat $c_{pa}T$ and latent heat Lq. The strong

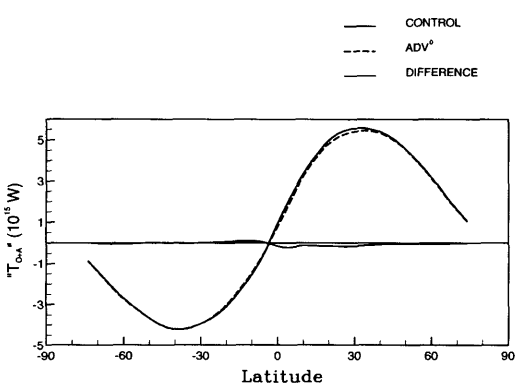

Fig. 15. Meridional integration of Fig. 13b (in 10^{15} W) which can be compared to T_A and T_O.

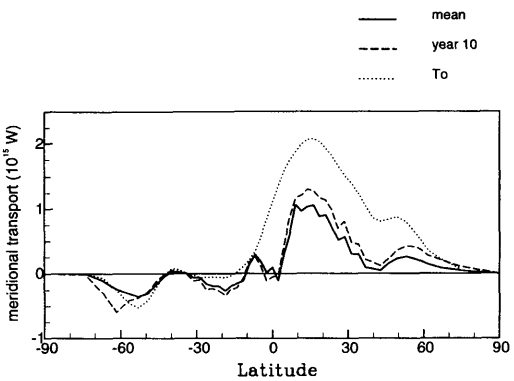

Fig. 16. Atmospheric transport in zonal and vertical mean: (a) curve *mean* (solid line) difference of T_A between ADV^0 and CONTROL for a 10-yr mean, (b) curve *year10* (dashed line) same as (a) but T_A for ADV^0, corresponds to the tenth year only (it is still a 10-yr mean for CONTROL). The term of ocean heat transport T_O is also represented (curve T_O in dotted line).

change in the transport of gz in the subtropical area corresponds to an acceleration of the Hadley cell mean circulation in ADV^0. This acceleration in turn introduces an increase in the sensible and latent heat transport equatorwards. On average, the atmospheric poleward transport in the Hadley cell is increased, with a maximum at latitude 15°N (Fig. 14).

This increase in the poleward transport of energy propagates to higher latitudes. Near 30°N the transport of energy is increased slightly and this increase mainly corresponds to an increased transport of sensible heat.

5. Conclusions

The partitioning of meridional heat transport between the ocean and the atmosphere is not well observed. When simulated in coupled atmosphere/ocean models, this fundamental feature of the Earth climate is known to be sensitive to some model parameterizations. In that study we have analyzed a simple experiment using an atmosphere/surface ocean coupled model where oceanic heat transport is prescribed.

The determination of the prescribed oceanic heat transport divergence used in the coupled model simulations is computed from the surface heat fluxes entering the ocean as simulated by the LMD atmospheric-only model forced with clima-

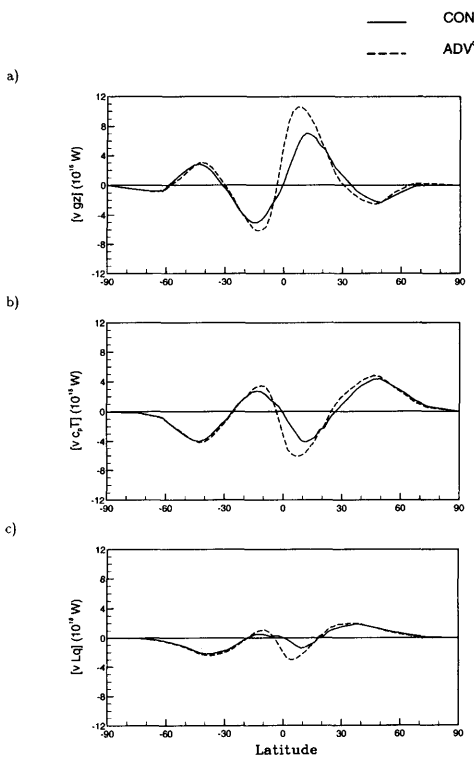

Fig. 17. Zonally and vertically integrated meridional transport of atmospheric energy (10^{15} W) by the total flow decomposed into (a) the transport of geopotential, (b) the transport of sensible heat and (c) the transport of latent heat. The solid curves represent the results of CONTROL and the dashed curves those of ADV^0, in average over the 10-yr simulations.

tological SSTs. The prescription of such an ocean heat advection term plays two functions which are deeply connected: A physical role which is to give in a simple manner the divergence of the heat transport by the oceanic currents, and a correction rôle to compensate, to the first order, the atmospheric model anomalies in the surface heat flux (Gaspar and Planton, 1990).

We suppress the ocean advection term and diagnose the effects of this on the atmospheric energetics. This study is meant as a way to foresee the range of errors that can result from erroneous ocean circulations in coupled ocean/atmosphere GCMs. We have concentrated our analysis on the first 10 years of the simulations, and we expect that some of the features we have determined will help us in diagnosing the initial drift in the complete atmosphere/ocean general circulation model under development in our laboratory.

While some of the results are not surprising, e.g., the low latitude temperature increase and the midlatitude temperature decrease, their amplitude and other associated characteristics of the atmospheric response are more difficult to predict. The atmospheric meridional heat transport is increased in the absence of the oceanic transport, with a maximum increase occuring exactly at the latitude of the maximum suppressed ocean transport. This compensating effect is of course partial and the meridional gradient of temperature remains larger in a climate without ocean heat transport, which is also a condition for the atmosphere transport to increase. But it is far from being negligible, and on the contrary, constitutes the dominant term during the period under consideration. This increased atmospheric transport and the reduced surface fluxes induce changes in the convective cloudiness in the ITCZ which tends to increase when the ocean circulation is suppressed: this modification constitutes both a consequence of the increased Hadley circulation and the manner chosen by the atmosphere to reduce (radiatively) the surface heat balance. This behaviour is reminiscent of the thermostat effect due to cirrus clouds described by Ramanathan and Collins (1991). It is of course dependent on the cloud parameterization of our atmospheric general circulation model. But we may expect the same processes to play a crucial role in the equilibrium of coupled dynamical ocean/atmosphere models.

6. Acknowledgements

We are grateful to Larry Gates and Peter Gleckler for their careful reading of the manuscript and their useful comments. We also acknowledge the comments of the two anonymous reviewers. This work was performed under the auspice of the CNRS (National Center for Scientific Research in France). Support for ECS was provided by the University of Versailles-St-Quentin-en-Yvelines and at LLNL (Livermore, USA), by the US Department of Energy Environmental Sciences Division, under Contract W-7405-ENG-48. The simulations were carried out at the IDRIS (Institut du Développement et des Ressources en Informatique Scientifique, Orsay, France) on a Cray 98.

REFERENCES

Adamec, D., Elsberry, R., Garwood, R. J. and Haney, R. 1981. An embedded mixed-layer-ocean circulation model. *Dynam. Atm. Oceans* **6**, 69–96.

Bennett, A. 1978. Poleward heat fluxes in southern hemisphere oceans. *J. Phys. Ocean.* **8**, 785–798.

Boer, G. 1986. A comparison of mass and energy budgets from two FGGE datasets and a GCM. *Mon. Wea. Rev.* **114**, 885–902.

Boer, G. J. 1993. Climate change and the regulation of the surface moisture and energy budgets. *Clim. Dyn.* **8**, 225–239.

Bryden, H. and Hall, M. 1980. Heat transport by currents across 25°N latitude in the Atlantic Ocean. *Science* **207**, 884–886.

Bryden, H. L., Roemmich, D. H. and Church, J. A. 1991. Ocean heat transport accross 24°N latitude in the Pacific. *Deep-Sea Res.* **38**, 297–324.

Carissimo, B., Oort, A. and Vonder Haar, T. 1985. Estimating the meridional energy transports in the atmosphere and ocean. *J. Phys. Ocean.* **15**, 82–91.

Chalita, S. and Le Treut, H. 1994. The albedo of temperate and boreal forest and the northern hemisphere climate: A sensitivity experiment. *Clim. Dyn.* **10**, 231–240.

Cohen-Solal, E. and Le Treut, H. 1996. Impact of ocean optical properties on seasonal SST: results with a surface ocean model coupled to the LMD AGCM, *Clim. Dyn.* **12**, 417–433.

Covey, C. 1988. Atmospheric and oceanic heat transport: simulations versus observations. *Climatic Change* **13**, 149–159.

Covey, C. and Thompson, S. L. 1989. Testing the effects of ocean heat transport on climate. *Palaeogeography, Palaeoclimatology, Palaeoecology* **75**, 331–341.

Ducoudré, N., Laval, K. and Perrier, A. 1993. SECHIBA, a new set of parameterizations of the hydrologic exchanges at the land-atmosphere interface within the LMD atmospheric general circulation model. *J. Climate* **6**, 248–273.

Esbensen, S. and Kushnir, V. 1981. The heat budget of the global ocean: an atlas based on estimates from surface marine observations. *Technical report 29*, Climatic Research Institute, Oregon State University.

Fouquart, Y. and Bonnel, B. 1980. Computations of solar heating of the earth's atmosphere: A new parametrisation. *Beiträge zur Physik der Atmosphäre* **53**, 35–62.

Fowler, L. D. and Randall, D. A. 1995. Liquid and ice cloud microphysics in the CSU general circulation model. Part 2: Impact on cloudiness, the Earth radiation budget, and the general circulation of the atmosphere. *J. Climate* **9**, 530–560.

Fu, L.-L. 1981. The general circulation and meridional heat transport of the subtropical South Atlantic determined by inverse methods. *J. Phys. Ocean.* **11**, 1171–1193.

Fu, L., 1986. Mass, heat and freshwater fluxes in the South Indian ocean. *J. Phys. Ocean.* **16**, 1683–1962.

Garwood, R. J. 1977. An oceanic mixed layer capable of simulating cyclic states. *J. Phys. Ocean.* **7**, 455–468.

Gaspar, P. 1988. Modeling the seasonal cycle of the upper ocean. *J. Phys. Ocean.* **18**, 161–180.

Gaspar, P. and Planton, S. 1990. Modelling the annual cycle of the ocean-atmosphere coupled system. *Annales Geophysicae* **8**, 1–10.

Gleckler, P. J. 1993. *The partitioning of meridional energy transport between the ocean and the atmosphere.* Ph.D. thesis, University of California, Davis.

Gleckler P. J., Randall, D. A., Boer, G., Colman R., Dix, M., Galin, V., Helfand, M., Kiehl, J., Kitoh, A., Lau, W. Liang, X.-Z., Lykossov, V., McAvaney, B., Miyakoda, K., Planton, S. and Stern, W. 1995. Cloud-radiative effects on implied oceanic energy transports as simulated by atmopheric general circulation models. *Geoph. Research Letters* **22**, 791–794.

Gleckler, P. J. and Weare, B. C. 1996. Uncertainties in global ocean surface heat flux climatologies derived from ship observations, *J. Clim.*, in press.

Hastenrath, S. 1980. Heat budget of tropical ocean and atmosphere. *J. Phys. Ocean.* **10**, 159–170.

Hastenrath, S. 1982. On meridional heat transports in the world ocean. *J. Phys. Ocean.* **12**, 922–927.

Hibler III, W. 1979. A dynamic thermodynamic sea ice model. *J. Phys. Ocean.* **9**, 815–846.

Holopainen, E. and Fortelius, C. 1986. Accuracy of estimates of atmospheric large-scale energy flux divergence. *Mon. Weath. Rev.* **114**, 1910–1921.

Hsiung, J. 1985. Estimates of global oceanic meridional heat transport. *J. Phys. Ocean.* **15**, 1405–1413.

Laval, K., Sadourny, R. and Serafini, Y. 1981. Land surface processes in a simplified global circulation model. *Geophys. Astrophys. Fluid Dyn.* **17**, 129–150.

Le Treut, H. and Li, Z. X. 1991. Sensitivity of an atmospheric general circulation model to prescribed SST changes: Feedback effect associated with the simulation of cloud optical properties. *Clim. Dyn.* **5**, 175–187.

Le Treut, H., Li, Z. X. and Forichon, M. 1994. Sensitivity of the LMD general circulation model to greenhouse forcing: Analysis of the atmospheric feedback effects. *J. Climate* **7**, 1827–1841.

Levitus, S. 1982. Climatological atlas of the world ocean. *Professional paper* **13**. NOAA; U. S. Department of Commerce, Washington.

Lubin, D. 1994. The role of the tropical super greenhouse effect in heating the ocean surface. *Science* **265**, 224–227.

Masuda, K. 1988. Meridional heat transport by the atmosphere and the ocean. *Tellus* **40A**, 285–302.

Meehl, G. A. 1995. Climate sensitivity and cloud-albedo feedback in a global coupled ocean-atmosphere GCM. In: *Climate sensitivity to radiative perturbations: physical mechanisms and their validation* (ed. H. Le Treut).

Springer-Verlag, Berlin, Heidelberg, New York, 231–237.

Meehl, G. A. and Washington, W. M. 1995. Cloud albedo feedback and the super greenhouse effect in a global coupled GCM. *Clim. Dyn.* **11**, 399–411.

Michaud, R. and Derome, J. 1991. On the mean meridional transport of energy in the atmosphere and oceans as derived from six years of ECMWF analyses. *Tellus* **43A**, 1–14.

Michaud, R. and Lin, C. 1992. Monthly summaries of merchant ship surface marine observations and implications for climate variability studies. *Clim. Dyn.* **7**, 45–55.

Morcrette, J.-J. 1991. Radiation and cloud radiative properties in the European Centre for Medium Range Weather Forecasts forecasting system. *J. Geoph. Res.* **96**, 9121–9132.

Oort, A. and Peixoto, J. 1983. Global angular momentum and energy balance requirements from observations. *Adv. Geophys.* **25**, 355–490.

Paulson, C. and Simpson, J. 1977. Irradiance measurements in the upper ocean. *J. Phys. Ocean.* **7**, 952–956.

Ramanathan, V. and Collins, W. 1991. Thermodynamic regulation of ocean warming by cirrus clouds deduced from the 1987 El Niño. *Nature* **351**, 27–32.

Randall, D. A., Fowler, L. D. and Dazlich, D. A. 1995. Cloud effects on the ocean surface energy budget. In: *Climate sensitivity to radiative perturbations: physical mechanisms and their validation* (ed. H. Le Treut). Springer-Verlag, Berlin, Heidelberg, New York, 239–249.

Roemmich, D. 1987. Estimation of meridional heat flux in the North Atlantic by inverse methods. *J. Phys. Ocean.* **10**, 1972–1983.

Sadourny, R. and Laval, K. 1984. January and July performance of the LMD general circulation model. In: *New perspectives in climate modelling* (ed. A.Berger and C.Nicolis). Elsevier, Amsterdam, 173–197.

Savijärvi, H. 1988. Global energy and moisture budgets from radiowind data. *Mon. Wea. Rev.* **116**, 417–430.

Schutz, C. and Gates, W. L. 1972. Supplemental global climatic data: January. *Technical report* **R-915**/1-ARPA, The Rand Corporation, Santa Monica, California USA.

Semtner, A. 1976. A model for the thermodynamic growth of sea ice in numerical investigations of climate. *J. Phys. Ocean.* **6**, 379–389.

Slingo, A. and Slingo, J. M. 1988. The response of a general circulation model to cloud longwave radiative forcing. I: Introduction and initial experiments. *Q. J. R. Meteorol. Soc.* **114**, 1027–1062.

Trenberth, K. E. and Solomon, A. 1994. The global heat balance: heat transports in the atmosphere and ocean. *Clim. Dyn.* **10**, 107–134.

Washington, W. M. and Meehl, G. A. 1993. Greenhouse sensitivity experiments with penetrative cumulus convection and tropical cirrus albedo effects. *Clim. Dyn.* **8**, 211–223.

Wunsch, C. and Hu, D. 1983. Mass, heat, salt and nutrient fluxes in the South Pacific ocean. *J. Phys. Ocean.* **13**, 725–754.